UKAEA-CCFE-PR(20)114

K. K. Kirov, E. Belonohy, C. D. Challis, J. Eriksson, D. Frigione, L. Garzotti, L. Giacomelli, J. Hobirk, A. Kappatou, D. Keeling, D. King, E. Lerche, P. J. Lomas, M. Nocente, C. Reux, F. G. Rimini, A. C. C. Sips, D. Van Eester, JET Contributors

Analysis of the fusion performance, beam-target neutrons and synergistic effects of JET high performance pulses

Analysis of the fusion performance, beam-target neutrons and synergistic effects of JET high performance pulses

K. K. Kirov, E. Belonohy, C. D. Challis, J. Eriksson, D. Frigione, L. Garzotti, L. Giacomelli, J. Hobirk, A. Kappatou, D. Keeling, D. King, E. Lerche, P. J. Lomas, M. Nocente, C. Reux, F. G. Rimini, A. C. C. Sips, D. Van Eester, JET Contributors

This is a preprint of a paper submitted for publication in Nuclear Fusion

Analysis of the fusion performance, beam-target neutrons and synergistic effects of JET high performance pulses

K. K. Kirov[1], E. Belonohy[1], C. D. Challis[1], J. Eriksson[2], D. Frigione[3], L. Garzotti[1], L. Giacomelli[4], J. Hobirk[5], A. Kappatou[5], D. Keeling[1], D. King[1], E. Lerche[6], P. J. Lomas[1], M. Nocente[7], C. Reux[8], F. G. Rimini[1], A. C. C. Sips[9], D. Van Eester[6] and JET Contributors*

EUROfusion Consortium, JET, Culham Science Centre, Abingdon, OX14 3DB, UK.
[1]CCFE Fusion Association, Culham Science Centre, Abingdon, OX14 3DB, UK.
[2] Department of Physics and Astronomy, Uppsala University, SE-75120 Uppsala, Sweden
[3] Unità Tecnica Fusione—ENEA C. R. Frascati—via E. Fermi 45, 00044 Frascati (Roma), Italy
[4] IFP-CNR, via R. Cozzi 53, 20125 Milano, Italy
[5] Max-Planck-Institut für Plasmaphysik, D-85748 Garching, Germany
[6] Lab. for Plasma Phys. KMS-ERM Renaissancelaan, 30 Avenue de la Renaissance B-1000, Brussels, Belgium
[7] University Milano-Bicocca, piazza della Scienza 3, 20126 Milano, Italy
[8] CEA, IRFM, F-13108 Saint Paul Lez Durance, France
[9] European Commission, B-1049 Brussels, Belgium

Abstract: Achieving high neutron yields in today's fusion research relies on high power auxiliary heating in order to attain required core temperatures. This is usually achieved by means of high Neutral Beam (NB) and Radio Frequency (RF) power. Application of NB power is accompanied by production of fast beam ions and associated Beam-Target (BT) reactions. In standard JET operational conditions, the latter and thermal fusion reactions are of the same order of magnitude. This study addresses important issues regarding the impact of density, central electron and ion temperatures and their ratio, T_i/T_e, on the fusion performance, measured by total neutron yield and BT neutron counts. NB/RF synergistic effects are discussed as well. It is demonstrated that while thermal reactions can be extrapolated based on existing scaling expressions, the BT neutrons are more difficult to predict and this task in general would require numerical treatment. In this study BT neutrons in JET best performing baseline and hybrid pulses are analysed and underlying dependencies discussed. Central fast ions densities are found to decrease with increased density and density peaking. This is attributed to poorer beam penetration at high density. The BT reactions however are unchanged and can even increase if operating at higher core temperatures. Increase in central ion temperature and T_i/T_e ratio leads to higher total and BT reaction rates as in the same time whilst simultaneously BT to total neutron ratio decreases significantly. NB/RF synergistic effects are found to have negligible impact on total neutron rate. This can be explained with reduced beam penetration in conditions of high density leading to lower central fast ions density.

* See the author list of E. Joffrin et al. 2019 Nucl. Fusion 59 112021

1 Introduction

Future fusion reactors must rely greatly on thermal nuclear reactions [1, 2]. The optimum temperature to achieve high thermal yield in DT plasma mixture is of the order of few tens of keV. Nearly all present research tokamaks use high power Neutral Beam Injection (NBI) to heat the plasma [3] and reach the temperatures necessary to sustain both high fusion gain and thermal nuclear yield. The application of NBI power is always accompanied by producing large amount of fast beam ions and associated reactions between themselves on the one hand and with the background target plasma on the other [4]. The former is known as the so-called Beam-Beam reactions and its contribution is usually small, while the latter is referred to as Beam-Target (BT) fusion reactions and it is usually of the order of the thermal reactions.

While the thermal rates can be projected based on the available scaling laws [5], [6], [7], BT rates cannot be easily predicted or extrapolated. This is due to the fact that beam deposition and fast ions densities depend comprehensively on atomic processes as well as on target plasma parameters. Beam penetration for instance depends on plasma density and profile peaking. Beam slowing down on the other side depends on electron temperature [8], [9], [46]. Target plasma ion temperature has a direct impact on BT rates [10], [11]. Therefore, these parameters must be included self-consistently in the analysis of BT reactions.

Understanding the contribution BT reactions to JET Deuterium – Deuterium (DD) neutron rates has been discussed in recent review paper [12]. The importance of separation of RF, NBI and thermal contributions by means of available diagnostics and analysis tools has been highlighted. It has been assessed [12], [13] that depending on the operating scenario between 40% to 60% of DD reactions in high performance pulses originate from BT reactions. Early JET Deuterium – Tritium (DT) experiments have estimated [14] that the contribution of the BT reactions accounts for about 50% of the total neutrons.

In presence of high power Radio Frequency (RF) heating under conditions where fast ions are in resonance with RF wave there could be strong interaction between both, RF wave and beam fast ions, resulting in more energetic particles production, changes to fast ions distribution function and BT fusion reaction rates. This is usually referred to as NB/RF synergistic effects and it has been shown that they have an impact on DD neutrons during previous JET campaign [15], [16], [17].

JET's scientific program in the last few years has mainly focussed on various issues in preparation for the forthcoming DT campaign: the physics basis for the DT operational scenarios, including the fusion power predictions through first principles and integrated modelling, and the impact of isotopes in the operation and physics of DT plasmas. In order to achieve the fusion power target of 15 MW for 5 s [18] the NB system has been upgraded to be able to deliver up to 35MW. Further to this higher fusion performances, i.e. increased fusion neutron yield, have been achieved by means of using low gas injection rate and applying high heating power, thus accessing lower collisionality regime in the core and achieving lower neutral pressure and high rotation at the H-mode pedestal. Lower collisionality helps decoupling the core ion and electron temperatures, T_i and T_e, and operating in higher T_i/T_e regime provides a positive feedback on the stabilisation of the ion temperature gradient turbulence. The positive feedback is stronger at high rotation, which is enabled by low gas injection [13].

Two complementary operational scenarios have been developed at JET as main candidates for sustained high DT fusion power [6], [19]: the standard H-mode scenario, also referred to as baseline scenario, with normalised beta and edge safety factor, $\beta_N \approx 1.8$ and $q_{95} \approx 3$ [20], and the hybrid scenario [21] with $\beta_N \approx 2–3$ and $q_{95} \approx 4$ [21]. The baseline scenario development [19] concentrates mainly on pushing the operation towards the high current and field limits with a relaxed current profile, whereas the hybrid experiments focus mainly on the advantages of operating at high β_N with a shaped current profile and central safety factor above 1.

The baseline scenario, which usually operates at lower β_N and higher plasma density domain, benefits from larger thermal neutron rates. JET's beam penetration is quite peripheral in this case affecting the contributions of BT reactions. In the hybrid scenario, which operates at lower densities allowing for central beam deposition, enhanced fusion performance is achieved by substantial BT rates achieved by the higher penetration of the neutral beams to the plasma core and a reduced ion temperature gradient turbulence by fast ions when electromagnetic effects are taken into account [22], [23]. In addition, high β_N regimes which aim at achieving higher neutron fluency would account even higher BT to total neutrons ratio. In all these scenario central density and density peaking are important as they will determine beam penetration. Plasma temperature on the other hand will have an impact on beam fast ions slowing down and thus will determine their density.

Studying the impact of electron density profiles peaking is essential regarding understanding their effect on BT and total neutron counts. It was noted [6] that density peaking could have an impact on ITER performance including energy confinement and fusion power production. A flat density profile is usually assumed [24] in the present ITER design, although, as shown in [25], moderately peaked density profiles due to the anomalous inward pinch can be expected according to predictions from the transport models [26]. It has been stipulated that if a peaked density profile can be sustained in ITER due to an inward pinch even with edge particle fuelling, higher fusion gain will be achieved [6].

The ratio of ion to electron temperature, T_i/T_e, is not only important regarding understanding better the suppression of ITG/TEM transport but also in extrapolating to burning plasma experiments where T_i/T_e is expected to be less than or equal to unity [6]. It should be noted that in DT plasma main heating by alpha particles will provide different power input to electrons and ions thus changing the ratio T_i/T_e measured in DD plasma. In the present analysis this parameter will not be studied with respect to its role on ion heat transport but rather its impact on the fusion performance. Both T_e and T_i are important contributors: DD thermal fusion rates scale as $\propto T_i^{2.12}$ in the region of typical tokamak operation, 1-20keV, and T_i is also having an impact on BT rates particularly for lower fast ions energies. The electron temperature, T_e, on the other side is directly responsible for NB ions slowing down thus affecting fast ions densities and hence has a significant impact on BT rates.

The impact on T_i/T_e on JET fusion performance has been studied in [13] with main focus on the thermal rates. Observed high fusion yield has been attributed to the decrease in collisionality and the increases in ion heating fraction in the discharges with high NB power. It has been noted that achieving $T_i > T_e$ regime of operation can also be attributed to positive feedback between the high T_i/T_e ratio and stabilisation of the turbulent heat flux resulting from the ion temperature gradient driven mode. It has been shown that BT rates were comparable [13] to thermal rates but the impact of T_i, T_e and their ratio on BT rates has not been covered in this study.

While the importance of these parameters, i.e. density profile peaking, electron and ion temperature and their ratio T_i/T_e, β_N, collisionality and normalised gyroradius, in transport and stability analysis is highlighted in numerous studies their impact on fusion performance and BT rates has rarely been studied. Indeed, the available scaling laws which allow us to extrapolate the fusion performance only account for the thermal energies and thermal fusion rates. On the other side, as it is highlighted here the BT rates provide significant contribution to JET DD [12] and DT [14] fusion performance. The impact of β_N, central density and density peaking and T_e/T_i on neutron yield is studied here by means of finding relationship between measured neutrons and these parameters. When BT neutrons and rates are considered TRANSP code was used to calculate the latter and extract underlying dependencies. TRANSP is further used when assessing the impact of these parameters on synergistic effects.

The purpose of this paper is to study the impact of central density and density profiles peaking, central electron and ion temperature and their ratio on the fusion performance, BT rates and synergistic effects. In assessing the impact of density profiles peaking the density peaking factor term, which is the ratio of electron density at normalised toroidal flux radius of 0.2 and 0.8, is used throughout in the paper. This study is not comprehensive overview of all possible factors and parameters that might impact on BT rates, but instead an attempt to provide an account on observed dependencies in high performance DD plasma. A large database of best performing baseline and hybrid scenario pulses with neutron counts exceeding $1x10^{16}$ 1/s during the latest JET campaign is used.

Paper is organised as follows. In section 2 details of modelling tools used in the study are provided. Diagnostics used in the study and brief description of typical pulse trends are discussed in chapter 3. Validation of the analysis versus available diagnostics is addressed in section 4. Results of the analysis is provided in section 5. Conclusions and prospects are presented in the last section of the paper.

2 Modelling tools used in the study

Analysis by means of TRANSP [27], [28], [29], [30] code is used in this study as emphasis is given to having neutron yield predicted as accurately as possible. In addition, diamagnetic measurements of the plasma energy are used as a constraint to the analysis. Matching both the neutron rates and plasma energy is in general challenging task in this type of analysis but it is essential [13] as it provides the necessary validation of the modelling results and backs up the conclusions from the numerical analysis. In addition, TRANSP is used to provide fast ions distribution functions and estimates of the BT and thermal neutron production rates as well.

The NUBEAM code [31] is a computationally comprehensive Monte-Carlo code for NB injection in tokamaks. The code follows the fast ion guiding centre trajectories, applying a finite Larmor radius correction and takes into account orbit effects in fast ion distribution calculations. The principal RF wave solver for TRANSP is the TORIC code [32]. To study the ion cyclotron (IC) resonance of the heated ions, Monte Carlo quasi linear RF kick operator [33], [34] implemented in NUBEAM was used in the study. The RF wave solver in TRANSP, TORIC, provides information about RF electric field components and perpendicular wave vector for each toroidal mode. RF resonance condition for a given harmonic is then used to calculate the magnetic moment and energy of the particles satisfying the resonant condition. Assuming that the resonant ions lose their phase information with RF wave by collisions and wave stochasticity before they re-enter the resonance layer, a random walk model can be used to reproduce the stochastic nature of RF heating in magnetic moment space. Every time fast ion passes through resonance layer it receives a kick in magnetic moment space. The magnitude of the kick is derived from the quasi-linear theory, while the stochastic nature is reproduced by means of Monte Carlo random number for the phase of the gyro-orbit. Details of the implementation of RF kick operator in NUBEAM code and results of various benchmarking tests are provided in [35]. At present there is no feedback from NUBEAM's fast ion distribution function to TORIC.

3 Experimental setup

3.1 Essential diagnostics

Experimental data from standard JET diagnostics and recommended signals were used in the study. Electron density profiles and temperature profiles were taken from the High Resolution Thomson Scattering diagnostics, HRTS, and/or LIght Detection And Ranging, LIDAR, measurements [36]. Electron temperature from ECE radiometer [37] was also included in the analysis. Radiated power was measured by the bolometric diagnostics [38], while Z_{eff} was assessed by means of Bremsstrahlung measurements from visible spectroscopy. Neutron production counts were taken from the available neutron yield monitors [39].
After the change of JET wall from C to Be and W metallic ITER Like Wall (ILW) traditional charge-exchange spectroscopy for T_i measurements, heavily relying on CVI spectra analysis, has become considerably more difficult. A combination of diagnostics was used to deduce T_i for the investigated pulses: X-ray crystal spectroscopy (XCS), Charge eXchange Recombination Spectroscopy (CXRS) [40] and neutron spectrometer.

3.1.1 JET neutron spectrometer TOFOR

Data from JET neutron Time-Of-Flight spectrometer (TOFOR) were used in the neutron spectra analysis and to validate TRANSP results. The TOFOR diagnostic is described in detail in [41, 42]. It has a vertical line of sight through the plasma core and perpendicular to the magnetic field covering the region between $2.74m<R_{maj}<3.02m$. TOFOR consists of two sets of plastic scintillator detectors. First is placed in the collimated flux of neutrons from the plasma and the second is placed 1.2 meters away at an angle of 30 degrees to the collimator line-of-sight. A fraction of the incoming neutrons scatter in the first detector and then some of them are detected by the second one. The time of each scattering event is recorded and from the two arrays of scattering times a time-of-flight (TOF) spectrum is constructed. The energy of incoming neutrons is determined by the TOF related to the measured distance between the two detectors. DD neutrons, which typically have energies of about 2.5 MeV, give rise to flight times around 65 ns. The full response function of TOFOR has been calculated with Monte-Carlo methods [43]. For the cases simulated and discussed here TOFOR time-resolution is a limiting factor; in order to obtain data with reasonable confidence one has to integrate over 0.5s around the time of interest.

Significant enhancement of beam-target neutron spectra by the RF power is expected for lower, $E_n<2MeV$, and higher energies, $E_n>2.8MeV$. Monoenergetic fast ions populations with energies of 100keV and 500keV would be expected to create double-humped shaped neutron spectra with high-energy peaks at $E_n=2.8MeV$ and $E_n=3.5MeV$ respectively. These estimates of E_n correspond to $t_{TOF}=61ns$ and $t_{TOF}=55ns$ [43]. This constitutes the basis of detection of fast ions created by RF by means of the TOFOR diagnostic.

3.1.2 JET neutron camera

Details of JET's neutron emission neutron profile monitor are provided in [44]. The instrument comprises two cameras; the horizontal camera consists of 10 collimators for 10 viewing chords and containing detector channels 1-10, views the vertical profile, while the vertical camera, comprising 9 collimators and containing detector channels 11-19, views the horizontal (or radial) profile. Channels 11-14 feature smaller collimators compared to channels 15-19. This is due to the line of sight of the detector to the plasma which go through a triangular port plate.

3.2 JET high performance baseline and hybrid pulses

The baseline [6] development experiment on JET [19] features a number of high performing pulses at high plasma current and input power. Pulse #96482, figure 1 a), have the following parameters: 3.3T/3.5MA, $q_{95}\approx3.0$ and at the time of maximum performance, t≈12.5s line integrated density of $\approx2.15\times10^{20}m^{-2}$ (line averaged of about $7.6\times10^{19}m^{-3}$), central $T_{e0}\approx7.5$keV and T_i near the plasma core of about 9-10keV. NB power of about 29MW was applied at 7.5s. ICRH power in dipole phasing at 51.4MHz was ramped from 8.0s and reached its maximum of about 4.7MW half a second later for H minority heating with $X[H]=n_H/n_e\approx0.04$, while the bulk radiated power measured by the bolometric measurements was about 30% of the total input power. Gas dosing during the main heating phase was $\approx1.0\times10^{22}$ el/s. Small pacing pellets were fired with frequency between 25 Hz and 45Hz to maintain plasma density and sustain regular ELMs. Type I ELMs with frequency of about 40Hz were observed from about 8.3s up until ≈14.5s. The pulse featured reasonable confinement with H98≈1.0, relatively high normalised beta, $\beta_N\approx1.8$, and record peak neutron count of about $4.1\times10^{16}s^{-1}$. The pulse was modelled in TRANSP and by JETTO from the start of the main heating phase, 7.5s, up until 14.5s.

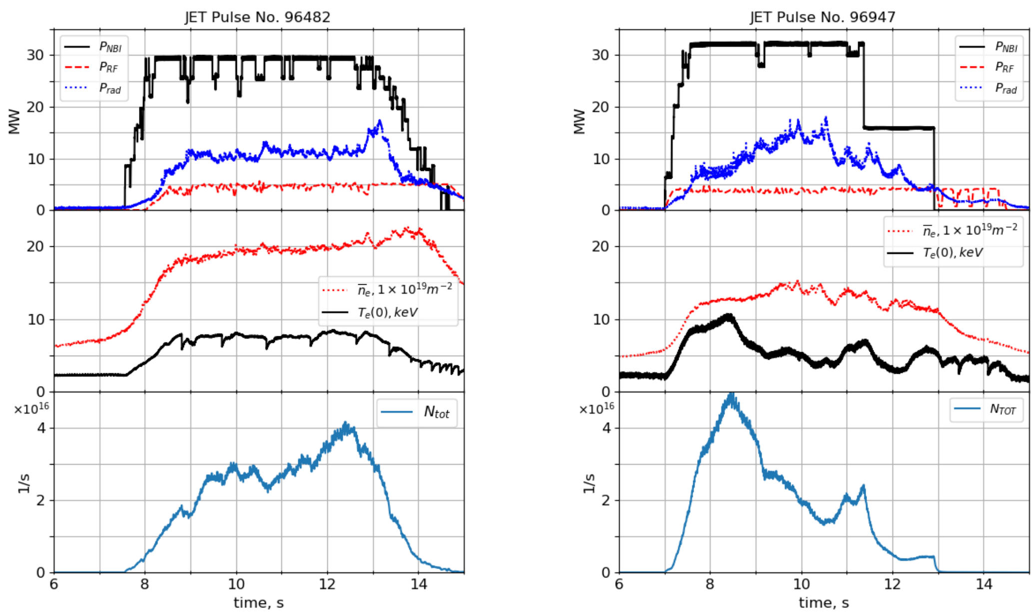

a) b)

Figure 1: a) Time traces of JET pulse #96482, 3.3T/3.5MA high performance baseline, top to bottom, P_{NB}, P_{RF} and bulk radiated power P_{rad}, line integrated density and central electron temperature, total neutron count; b) same as a) but for JET pulse #96947, 3.4T/2.25MA high performance hybrid.

JET pulse #96947, figure 1 b), was the best performing hybrid scenario with record peak neutron yield during the last JET campaign, up until March 2020. The pulse was carried out as part hybrid scenario development experiment and its main parameters are as follows: 3.4T/2.25MA, line integrated density ≈$1.3 \times 10^{20} m^{-2}$ rising up to ≈$1.5 \times 10^{20} m^{-2}$ (line averaged of about $4.6\text{-}5.3 \times 10^{19} m^{-3}$), central T_{e0}≈10keV at the time of highest neutron yield, and T_i near the core, normalised minor radius of about 0.2, of about 11.5keV were achieved by means of 32.3MW of NBI power and 4MW of ICRH in dipole phasing at 51.4MHz for H minority heating. Gas dosing during the main heating phase was about 8×10^{21} el/s maintaining steady ELMs while the target H minority concentration was kept at about $X[H]=n_H/n_e \approx 0.045$. Confinement was of the order of H98≈1.33 for about 1s from the start of the main heating. Normalised beta $\beta_N \approx 2.0$ was sustained during high performance phase, while neutron yields up to $4.9 \times 10^{16} s^{-1}$ were measured, which is one of the highest for JET with ITER-like wall. Performance deteriorated after 8.5s due to n=3 MHD mode triggered by fishbone activity followed by impurity accumulation and radiation peaking.

A summary of main plasma parameters from high-performance baseline and hybrid pulses averaged over 1s during high fusion phase are shown in Table 1. Almost all high performing JET pulses have a similar time evolution. At the end of current ramp-up phase for the baseline pulses, or in hybrid scenario at the end of the current ramp down after the current overshoot phase, high NB and RF heating power is applied. Entrance to H-mode and first ELM timing differ for different scenario and from pulse to pulse. This is because in large number of pulses optimisation of the large initial gas puff before main heating phase was attempted. High temperatures build in about 0.5s to 1s after power switch on and then high-performance phase begins. It is characterised with very high neutron yields, usually above 1×10^{16} 1/s. Gas injection from gas introduction modules is usually kept low to achieve enhanced performance in low collisionality regime. At the same time a real-time feedback on the main gas injection was used in hybrid pulses and pellets injection in baseline pulses in order to control the ELM frequency. During this steady phase before impurity to start accumulating and radiation to begin to increase, the core electron density increases steadily together with central ion and electron temperatures. Density peaking usually increases as well during this phase therefore density peaking factor and core temperatures are often correlated. Later high radiation events are observed followed rapidly by mid-Z impurities accumulation in the plasma core. This is usually consequence of ELMs frequency decrease and deteriorating ability of the ELMs to flush out impurities from plasma periphery. Once the radiation peaks and reaches high value the performance is lowered. Impurity accumulations are usually accompanied by very large density peaking so in the following analysis data from such events are excluded.

Table 1. Main parameters of high-performance baseline and hybrid pulses averaged over 1s during high fusion phase.

Pulse #	Bt, T	Ip, MA	P_{NBI}, MW	P_{RF}, MW	P_{RAD}, MW	W_{DIA}, MJ	R_{NT}, 1/s	R_{INJ}, el/s	Zeff
baseline pulses									
96480	3.3	3.5	29.0	4.6	10.7	8.7	2.30E+16	1.10E+22	1.64
96481	3.3	3.5	24.6	4.6	10.1	8.3	2.10E+16	1.10E+22	1.71
96482	3.3	3.5	29.0	4.7	11.1	9.9	3.50E+16	1.10E+22	1.78
96486	3.3	3.5	27.2	3.8	9.2	8.2	2.00E+16	1.10E+22	1.58
hybrid pulses									
95956	2.8	2.2	25.9	4.3	8.0	6.7	2.14E+16	1.18E+22	2.04
95964	3.4	2.2	28.0	4.4	9.2	6.4	2.29E+16	1.52E+22	2.31
96435	3.4	2.2	27.7	5.0	10.8	7.6	3.29E+16	1.00E+22	2.12
96947	3.4	2.3	31.8	3.7	6.5	8.1	3.56E+16	1.15E+22	1.69

In the pulses analysed here, time slices are taken from high performance phases, i.e. between 1s after heating phase starts and impurity accumulation event. The latter is assessed by central electron temperature trends or time of significant increase in radiated power. In some cases, when the steady state phase of a pulse is longer, e.g. more than 1s, multiple time slices from this pulse are analysed.

4 Validation of TRANSP runs

The conclusions in this study are greatly based on the results from TRANSP interpretative analysis. The validation of this analysis includes comparing the data from the modelling to the available measurements. Usually predicted neutron counts and plasma energy from TRANSP are routinely compared to the relevant diagnostics [13], [17]. In addition, a number of supplementary checks are used in our approach. Two additional synthetic diagnostics, neutron spectrometer and neutron camera, are used to cross check that the predicted fast ions distribution function and neutron emissions are consistent with the measurements.

Results for measured versus calculated total neutron count and plasma energy for all high-performance cases are shown in figure 2.

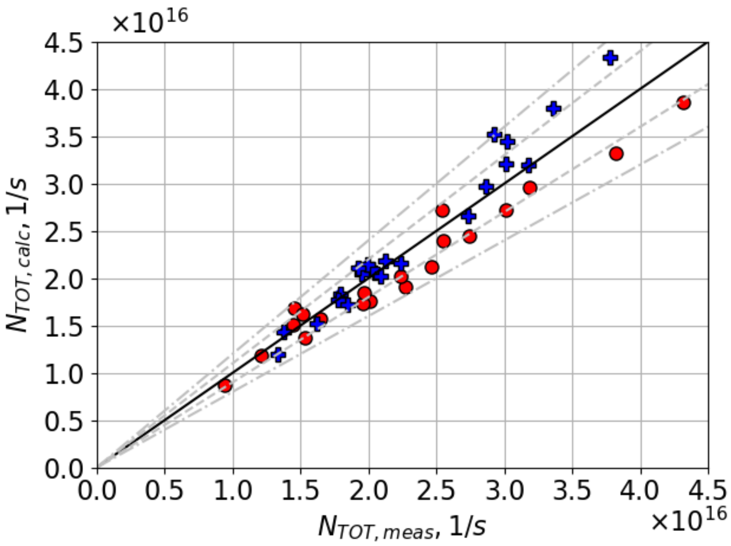

Figure 2: Calculated $N_{TOT,calc}$ vs. measured $N_{TOT,meas}$ total neutron counts for all recent JET high performance pulses. Baseline pulses are in blue crosses, whilst hybrid pulses are in red circles. The deviation of the calculated data from the measurements by 10% and 20% are shown by grey dashed and dash-dotted lines respectively.

The calculated neutron counts in figure 2 are in a very good agreement with measurements. With small number of exceptions, nearly all calculations are within 10% of measured values. For high performing pulses with total neutrons larger than $2.5x10^{16}$ 1/s the calculated neutrons for the baseline pulses are slightly higher than the measured, while for the hybrid pulses the calculated values are in general slightly lower than the measured.

Plasma energy measured by the diamagnetic diagnostic is compared to the calculated plasma energy in figure 3, showing that calculated and measured plasma energy are also in a good agreement.

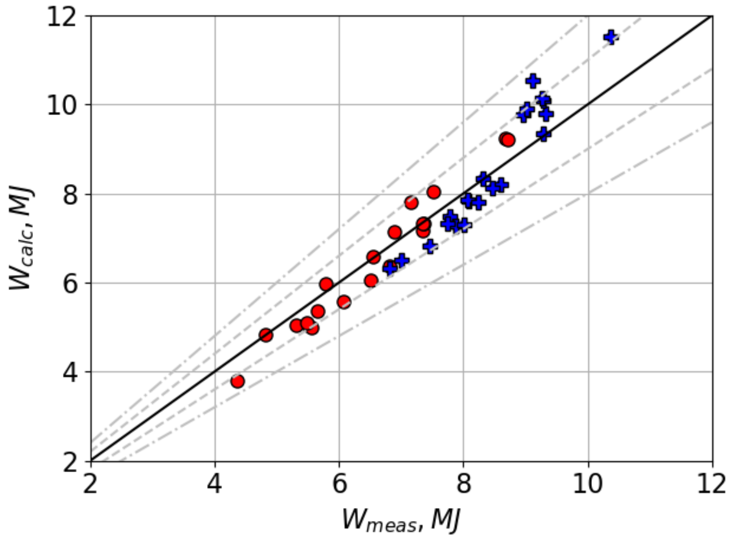

Figure 3: Calculated W_{calc} vs. measured via diamagnetic measurements W_{meas} plasma energy. Baseline pulses are in blue crosses, whilst hybrid pulses are in red circles. The deviation of the calculated data from the measurements by 10% and 20% are shown by grey dashed and dash-dotted lines respectively.

Differences in calculated energy versus measured are slightly higher for high performing baseline pulses with few cases with larger than 10% but not exceeding 16%. Noting that in general achieving great consistency between measured and calculated total neutron count and plasma energy in TRANSP is challenging task, one can conclude that the presented simulations are in a very good agreement with experimental measurements.

Results from TOFOR analysis is shown in figure 4 where measured t_{TOF} is compared with the expected one.

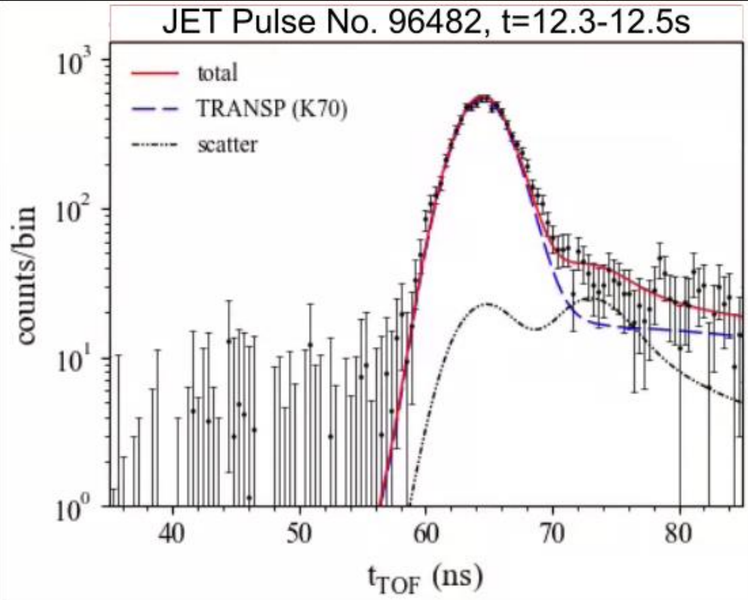

Figure 4: Neutron spectrum from TOFOR diagnostic for JET pulse #96482, 12.3-12.5s. Measured time-of-flight, t_{TOF} , (black points) is compared to total predicted (red) which is superposition of result from TRANSP fast ions distribution function (blue dashed line) and scattered neutrons (dash-dotted line).

Results of TOFOR analysis for pulse #96482 are shown in figure 4. Excellent agreement between measured spectrum and modelled one confirms that the fast ions distribution function provided by TRANSP is consistent with experimentally observed neutron spectra. The match of the shape of the neutron spectrum vs. time-of-flight for values of t_{TOF} between 60ns and 70ns provides additional certainty in calculated fast ions distribution function. One should note that the lack of significant neutron counts in the region 55ns-61ns indicates that RF synergy effects are possibly very small.

Neutron camera lines of sight and data from all 19 lines are provided in figure 5.

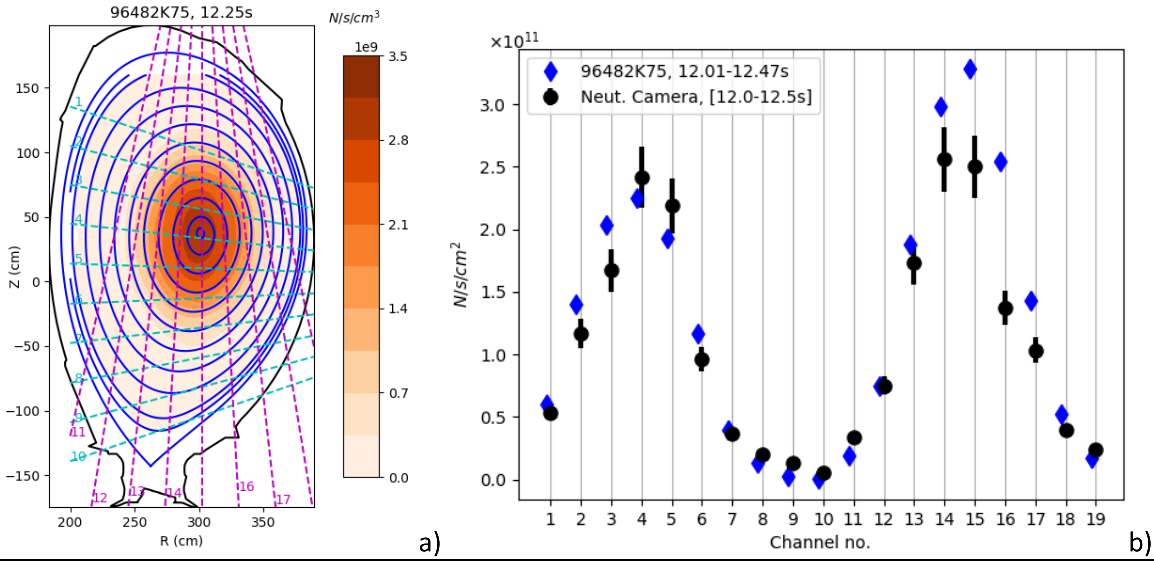

Figure 5: a) Neutron camera lines of sights for 10 horizontal and 9 vertical cannels. Provided is the plasma equilibrium and calculated neutron rates, $R_{TOT}(R,Z)$ in 1/s/cm^3, colour mapped in plasma cross-section for 96482K75, 12.25s. b) Neutron camera data for lines 1 to 19 (black) for pulse

#96482, averaged between 12s-12.5s. Results are compared to TRANSP run 96482K75 (blue points) where calculated neutrons were found to be over-calculated by about 15% of measured ones in the investigated time interval.

A very good agreement between the measured and calculated neutron fluxes has been observed on most of the channels, figure 5 b). The largest discrepancy is for channel 16 where TRANSP predicts about twice higher neutron fluxes. Another notable discrepancy is on channel 15 where calculated neutron flux is about 30% higher than the measurement. For the rest of the channels the match between measurements and calculations is very good. Inconsistent data for channels 14 to 16 have been also observed in previous studies [47]. One possible explanation noted in [47] could be due to incorrect or slightly misaligned Shafranov shift used in TRANSP. This however cannot explain the larger calculated neutron fluxes for all central vertical lines-of-sight observed here. Changes in collimators size, the viewing solid angle and the backscatter coefficients from the original calibrations [44] are possible explanations to the observed discrepancies.

5 Experimental results

JET's high performing baseline and hybrid pulses are analysed during their steady-state phase, which is the time interval starting 1 second after heating switch on and ending before impurities accumulation and radiation peaking followed by performance degradation. The impact of plasma parameters, electron density, n_e, and electron and ion temperatures, T_e and T_i, are studied by analysing these parameters in the plasma centre, i.e. at normalised toroidal flux radius ρ=0, in the core, ρ=0.2, and at the pedestal, ρ=0.8.

5.1 Total and thermal neutrons

5.1.1 Dependencies on core density and temperature

Total neutron counts are first studied versus core values of electron density and temperature and ion temperature. In these studies, 3.3T/3.5MA baseline pulses with fixed pedestal density and temperatures were used: $n_e(0.8)\approx5.5\times10^{19}m^{-3}$, $T_e(0.8)\approx1.5keV$ and $T_i(0.8)\approx2keV$. Results are shown in figure 6.

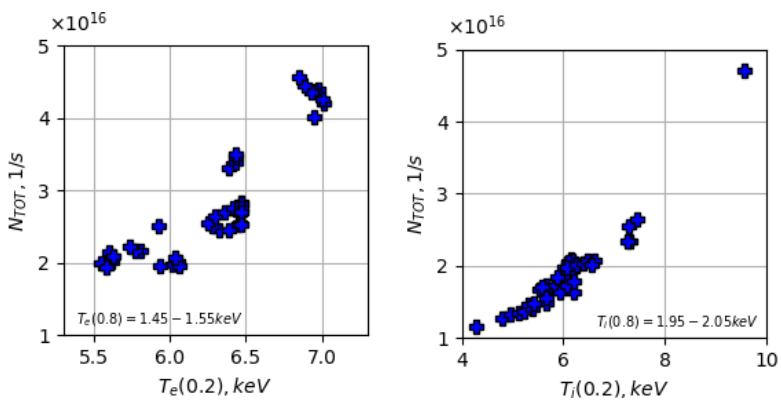

a) b) c)

Figure 6: Total neutron counts as calculated by TRANSP, N_{TOT}, versus electron density a) electron temperature b) and ion temperature c) in the core at ρ=0.2 for JET's high-performance 3.3T/3.5MA baseline pulses. The pedestal values, taken at ρ=0.8, are fixed and provided at the bottom of the graphs.

Performance, measured by the total neutron counts N_{TOT}, increases with core values of n_e, T_e and T_i, figure 6. Considering that the pedestal values of these parameters are fixed the above conclusion is also valid regarding N_{TOT} dependence on profiles peaking. Although it can be observed that fusion performance improves with density peaking, $N_{TOT}\approx1.75\times10^{16}$ 1/s for $n_e(0.2)/n_e(0.8)\approx1.44$ increasing to about 2.25×10^{16} 1/s for density peaking of 1.62 figure 6 a), care should be taken when making more general conclusion regarding fusion performance dependencies. As discussed in section 3.2 during the evolution of the high-performance pulses core density, density peaking and core temperatures increase simultaneously. This means that trends shown in figure 6 cannot be interpreted as direct dependencies of N_{TOT} on $n_e(0.2)$, $T_e(0.2)$ and $T_i(0.2)$ individually. Detailed analysis of the whole set of data shows that despite the negative impact of higher core density and density peaking on beam penetration the total neutrons and the fusion performance are in fact improved due to achieving higher core temperatures and thermal reactions.

JET's high-performance hybrid pulses in general follow the same trends. Since hybrid pulses are at lower density, $n_e(0.2)\approx5.8\text{-}6.4\times10^{19}$ m^{-3}, and benefit more from central beam penetration and consequent heating and fuelling one would expect significant drop in performance with increase in core density and density peaking. The density peaking factors of the hybrid pulses are comparable to those on the baseline pulses, $n_e(0.2)/n_e(0.8)\approx1.46\text{-}1.6$, and again the fusion performance was not affected by higher values of $n_e(0.2)/n_e(0.8)$. As with the baseline pulses, achieving higher core temperatures in hybrid experiments compensates for the reduced NB penetration and the outcome was higher fusion performance.

5.1.2 Triple product scaling with total and thermal neutrons

One of the most important figure of merit for the future fusion reactor is the fusion gain. The ratio of total neutron count to power losses, N_{TOT}/P_{LOSS}, is used here as an estimate of the fusion gain, P_{FUS}/P_{LOSS}, which is shown to be proportional to the triple product $\beta\ (B_t\tau)\ B_t$ [7], [48]. Using neutron counts, N_{TOT}, as a proxy for P_{FUS} follows from the fact that $P_{FUS} = (n_D/2)^2 \langle\sigma.v\rangle_{DD}\ Q_{FUS}$, where Q_{FUS} is the fusion energy released per 1 reaction. In DD plasma there are two possible nuclear reactions with nearly equal probability, hence one can use the neutron branch reaction and associated total neutron counts to assess P_{FUS}. The total neutron counts, N_{TOT}, can be replaced with thermal, N_{TH}, or BT neutrons, N_{BT}, which in turn can provide the contributions of the two main sources. In our analysis neutron counts are calculated by TRANSP and the agreement between the predictions and the measurements, figure 2 and 3, supports the conclusions. The code is also used to provide P_{LOSS}, which is a sum of conductive, convective and radiation losses as well as thermal energy confinement time, τ, and plasma thermal energy needed for β calculation.

Although the original expression, $P_{FUS}/P_{LOSS} \propto \beta\ (B_t\tau)\ B_t$, is strictly valid for DT plasma [7], where the DT reaction cross section is assumed approximately proportional to T_i^2, i.e. $\langle\sigma.v\rangle_{DT} \propto T_i^2$, it can be shown that it can be also applied for DD plasma as well. Indeed, the cross-section $\langle\sigma.v\rangle_{DD}$ of the neutron branch of DD reactions is approximately proportional to T_i^{α} where $\alpha\approx2.12$ in temperature range of interest, between 1keV to 20keV [10]. This allows for the use of the triple product, $\beta\ (B_t\tau)\ B_t$, to assess the fusion gain in DD plasma. Taking onto account that $\beta_N=\beta(aB_t/I_p)$ the triple product transforms into $\beta_N\ (B_t\tau)\ (I_p/a)$ and for pulses with same plasma current, I_p, only two parameters, β_N and $B_t\tau$, can be used to assess the fusion gain.

Assessing the fusion gain via the triple product relies on the assumption that $<\sigma.v>_{DT} \propto T_i^2$. While in general this is a rough approximation of the very strong dependence of fusion cross-section with T_i [10], in the temperature ranges of interest, 1keV to 20keV, the deviation of $<\sigma.v>_{DT}$ from T_i^2 dependence is small. The importance of this approximation and the impact of the density and temperature profiles have been discussed in [48], [49]. The impact of approximating $<\sigma.v>_{DT} \propto T_i^2$ for various density and temperature profiles has been assessed to result in errors in assessing the fusion power by maximum of about 20% for volume averaged ion temperatures between 5keV and 10keV [48].

In figure 7 shown is the ratio of neutron yield, N_{TH} for thermal and N_{TOT} for total, to power losses, P_{LOSS} versus β_N and $B_t\tau$. Data is collected from 3.3T/3.5MA high-performance baseline pulses. For the thermal neutrons, N_{TH}, the expected linear dependence can be seen from the plots of N_{TH}/P_{LOSS} vs. β_N and N_{TH}/P_{LOSS} vs. $B_t\tau$ shown in figure 7 b). The linearity of the dependences N_{TH}/P_{LOSS} vs. β_N at fixed $B_t\tau \approx 1.0$ in figure 7 b) left graph and N_{TH}/P_{LOSS} vs. $B_t\tau$ at fixed $\beta_N \approx 1.34$ in figure 7 b) right graph is shown by means of a least square fit of the data to a straight line. Parameters of the fit, slope *a* and residuals χ^2, are shown in the top left corner of the graphs. The fitted lines and the residuals, χ^2, show that the expected linear dependence of N_{TH}/P_{LOSS} with β_N and of N_{TH}/P_{LOSS} with $B_t\tau$ is fully consistent with scaling expressions as discussed in [7]. These trends are, however, more scattered from linear dependence when total neutron count, N_{TOT}, which has contributions from thermal and BT neutrons, is used, figure 7 c). Residuals of the least square fits of N_{TOT}/P_{LOSS} are 2.5-3 times larger than the ones related to N_{TH}/P_{LOSS} fits.

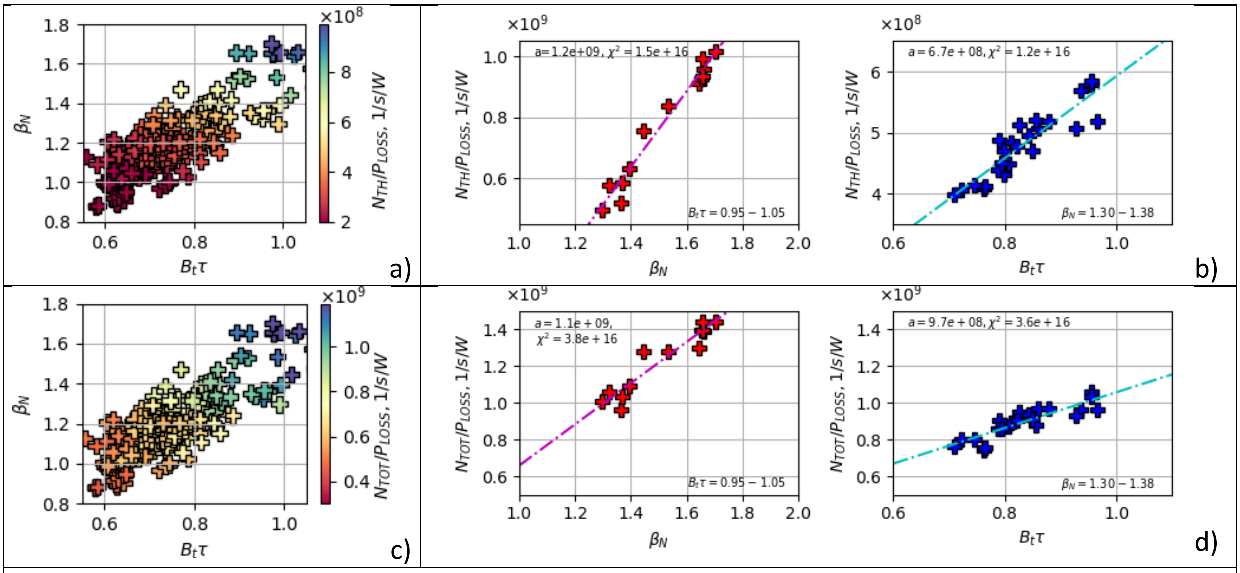

Figure 7: (top row) The ratio of the thermal neutron counts, N_{TH}, to power losses, P_{LOSS}, versus normalised beta, β_N, and product $B_t\tau$; (bottom row) The ratio of the total neutron counts, N_{TOT}, to power losses, P_{LOSS}, versus normalised beta, β_N, and product $B_t\tau$. From left to right shown is colour mapped symbols for N_{TH}/P_{LOSS} in a) and N_{TOT}/P_{LOSS} vs. β_N and $B_t\tau$ in c). N_{TH}/P_{LOSS} vs. β_N at fixed $B_t\tau \approx 1$ ($0.95 < B_t\tau < 1.05$) and on the right vs. $B_t\tau$ at fixed $\beta_N \approx 1.34$ ($1.3 < \beta_N < 1.38$) in b) and N_{TOT}/P_{LOSS} vs. β_N at fixed $B_t\tau$ and on the right vs. $B_t\tau$ at fixed β_N in d). Datapoints are from JET 3.3T/3.5MA high performance baseline pulses. Least square fit parameters, slope *a* and residuals χ^2, from the fits to straight lines (dash-dotted lines) are shown in top left corner of the graphs in b) and d).

The dependence of the fusion gain, assessed by means of the ratio N/P_{LOSS}, for the hybrid pulses is shown in figure 8. Thermal neutrons to lost power, N_{TH}/P_{LOSS}, is shown in figure 8 top row and it seems β_N dependence at fixed $B_t\tau \approx 0.65$ is as expected nearly linear, figure 8 b) left graph. On the other side, N_{TH}/P_{LOSS} vs. $B_t\tau$ at fixed $\beta_N \approx 1.7$ figure 8 b) right graph, is also nearly linear and very similar to the baseline case, figure 7 b) right graph. The total neutrons to power losses ratio, N_{TOT}/P_{LOSS}, is shown in figure 8 c) and d) and here again expected β_N and $B_t\tau$ dependencies are more scattered as the residuals to the fits show.

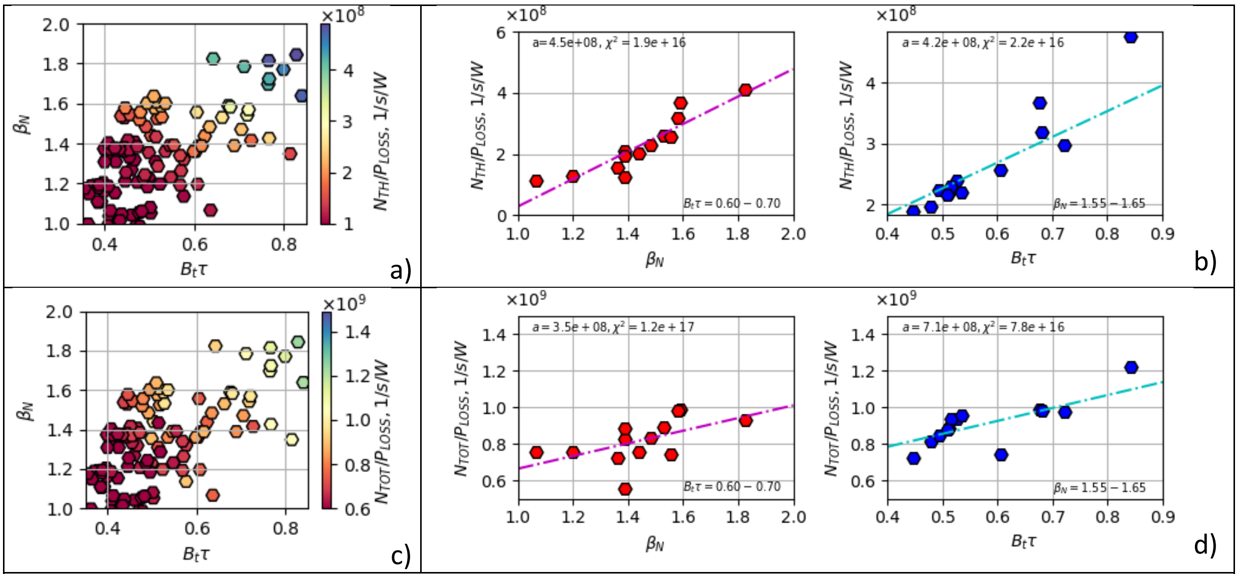

Figure 8: (top row) The ratio of the thermal neutron counts, N_{TH}, to lost power, P_{LOSS}, versus normalised beta, β_N, and product $B_t\tau$; (bottom row) The ratio of the total neutron counts, N_{TOT}, to lost power, P_{LOSS}, versus normalised beta, β_N, and product $B_t\tau$. From left to right shown is colour mapped symbols for N_{TH}/P_{LOSS} in a) and N_{TOT}/P_{LOSS} vs. β_N and $B_t\tau$ in c). N_{TH}/P_{LOSS} vs. β_N at fixed $B_t\tau \approx 0.65$ ($0.60 < B_t\tau < 0.70$) and on the right N_{TH}/P_{LOSS} vs. $B_t\tau$ at fixed $\beta_N \approx 1.6$ ($1.55 < \beta_N < 1.65$) in b) and N_{TOT}/P_{LOSS} vs. β_N at fixed $B_t\tau$ and on the right N_{TOT}/P_{LOSS} vs. $B_t\tau$ at fixed β_N in d). Datapoints are from 3.4T/2.2MA and 2.8T/2.2MA high performance hybrid pulses. Least square fit parameters, slope *a* and residuals χ^2, from the fits to straight lines (dash-dotted lines) are shown in top left corner of the graphs in b) and d).

From figures 7 and 8 one can conclude that while the thermal fusion follows very closely the predictions and is nearly linear with confinement and normalised beta, the contribution of the beam target reactions to the total fusion performance changes this picture. As a result, N_{TOT}/P_{LOSS} does not follow very closely the scaling laws. In the case that BT neutrons account for significant amount of the reactions it is important to understand the underlying dependencies. This is also essential in order to maximise fusion performance.

5.2 BT neutrons

5.2.1 Impact of central density

BT neutron yields are further analysed versus kinetic plasma profiles: n_e, T_e and T_i. Here emphasis is given to dependencies on the central values of n_e, T_e and T_i.

BT neutron counts are first analysed by studying the central fast ion density, $n_{fi}(0)$. The fast ions density is in general not poloidally symmetric, e.g. see fast ions density $n_{fi}(R,Z)$ in figure 14, therefore n_{fi} is only considered here at the plasma centre, i.e. $n_{fi}(0)$. Fast ions density central values, $n_{fi}(0)$, versus central electron density $n_e(0)$ for the baseline pulses are shown in figure 9 a). The corresponding BT counts, N_{BT}, are shown in figure 9 b). In order to discard possible correlation between central density and temperatures the database in figure 9 is limited to cases with central electron temperature of $T_e(0)$=6.6keV±5% or $T_e(0)$ in the range 6.3-6.9keV. This ensures that the observed trends are only due to central density variations.

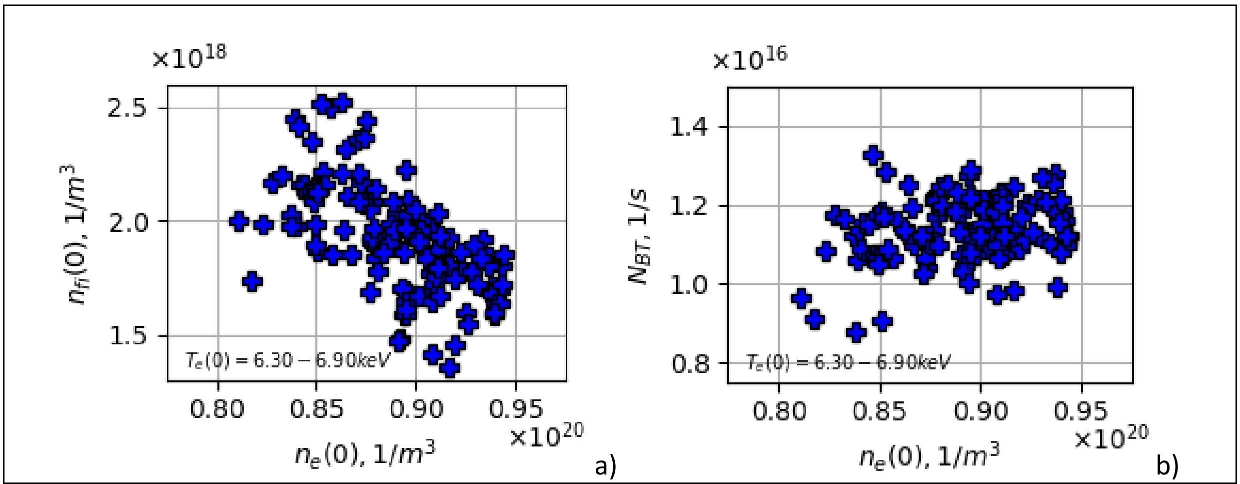

Figure 9: a) Central fast ions density, $n_{fi}(0)$, versus central electron density, $n_e(0)$, for JET's 3.3T/3.5MA high-performance baseline pulses; b) Total BT neutrons, N_{BT}, versus central electron density, $n_e(0)$. The subset of data is for central electron temperature in the range $T_e(0)$=6.3-6.9keV.

Central fast ions density, $n_{fi}(0)$, decreases, figure 9 a), with increasing central electron density $n_e(0)$ as beam penetration is reduced. Similar effect on the central fast ions density, $n_{fi}(0)$, has the electron density peaking. Despite this unfavourable trend of $n_{fi}(0)$ with $n_e(0)$ and density peaking, BT counts seem to not change significantly, figure 9 b). Central electron temperature in this database is fixed in the range $T_e(0)$=6.3-6.9keV which means that this parameter practically has no contribution in $n_{fi}(0)$ and N_{BT} trends. In addition there are no correlations between $n_e(0)$, $T_e(0)$ and $T_i(0)$ for the data set shown in figure 9. One possible explanation of the observed dependencies then is by means of geometrical effects associated with the larger volume of the plasma for off axis beam deposition. Indeed, by limiting the NB penetration and shifting the beam deposition to low field side (LFS) the fast ions density peaks at larger minor radius thus the increased volume at larger minor radius compensates for the reduces $n_{fi}(0)$.

Fast ions density central values, $n_{fi}(0)$, for the hybrid pulses are shown in figure 10 a). The corresponding BT counts, N_{BT}, are shown in figure 10 b). The database in figure 10 is restricted to central electron temperature of Te(0)=6.8keV±4% or $T_e(0)$ in the range 6.5-7.1keV.

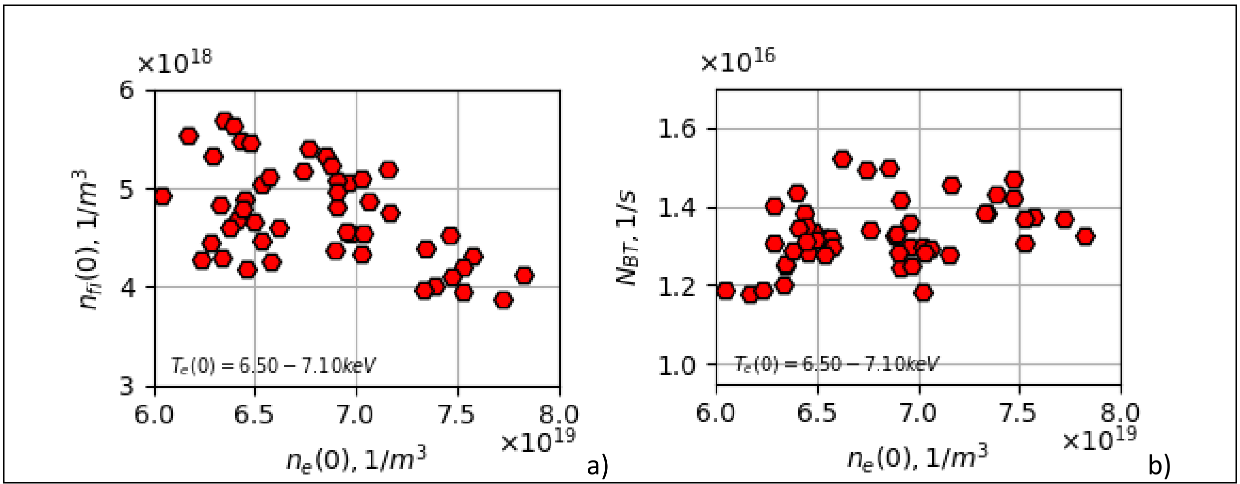

Figure 10: a) Central fast ion density, $n_{fi}(0)$, versus central electron density, $n_e(0)$ for JET's 2.15MA high-performance hybrid pulses; b) Total beam-target neutrons, N_{BT}, versus central electron density $n_e(0)$. The database is for central electron temperature in the range $T_e(0)$=6.5-7.1keV.

For the hybrid pulses central fast ions density, $n_{fi}(0)$, also decreases with central electron density $n_e(0)$, figure 10 a). Hybrid pulses are at lower density compared to baseline ones and beam deposition is usually more peaked on-axis. Small modifications to central electron density $n_e(0)$ will then have a significant impact on central fast ions density, $n_{fi}(0)$, as shown in figure 10 a). As with the baseline cases, BT neutrons do not change significantly with central density, figure 10 b). Here again the observed dependencies can be explained by means of geometrical effects associated with the larger volume of the plasma for off axis beam deposition.

From figures 9 and 10, it can be concluded that despite the reduction in beam penetration and central fast ions density with central electron density and peaking this has practically no effect on BT neutrons in the range of densities used in these experiments. Further analysis taking into account changes in central electron and ion temperatures shows that actually BT neutrons, N_{BT}, increase for higher values of $T_e(0)$ and $T_i(0)$ and this effect is not diminished by operating at higher $n_e(0)$ and density peaking.

5.2.2 Impact of T_i, T_e and their ratio

Here an account of the BT neutrons dependence on electron and ion temperature is provided. It is well known that increasing both T_e and T_i will have positive impact on BT counts [8], [9], [11]. The thermal neutron yield also increases strongly with T_i [10], so here the focus is on which of the two, BT and thermal neutrons, are affected more by operating at higher temperatures. This problem is addressed and answered in figure 11 where BT neutrons are plotted versus central $T_e(0)$ and $T_i(0)$.

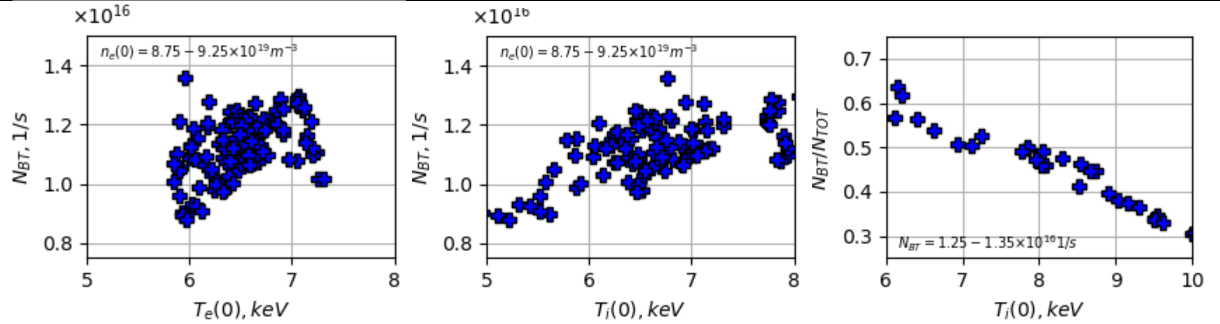

a) b) c)

Figure 11: BT neutrons, N_{BT}, versus central electron $T_e(0)$ a) and ion temperature $T_i(0)$ b) for 3.3T/3.5MA baseline pulses with $n_e(0)$=8.75-9.25×$10^{19}m^{-3}$ and the ratio of BT neutrons to total calculated neutrons, N_{BT}/N_{TOT}, for N_{BT}≈1.3e16 1/s in c)

For baseline pulses, N_{BT} increases with $T_e(0)$ and $T_i(0)$ for fixed central electron density, $n_e(0)$=9×$10^{19}m^{-3}$±3%, figure 11 a) and b). As the central electron and ion temperatures are usually very difficult to de-correlate in experiment, it is difficult to conclude here which of $T_e(0)$ and $T_i(0)$ has prevailing effect on N_{BT}. Electron temperature itself has no direct impact on thermal neutrons, while both thermal and BT fusion reaction cross-sections depend strongly on T_i. The main conclusion from figure 11 then will be that while increasing both $T_e(0)$ and $T_i(0)$ benefits N_{BT}, the most important contribution regarding the total fusion performance is on $T_i(0)$. Indeed, the thermal neutrons overtake the beam driven ones as seen in figure 11 c), where for fixed BT neutrons it is observed that the ratio N_{BT}/N_{TOT} decreases with increasing central ion temperatures. Our analysis shows that in this case while the BT counts are up by few tens of per cents, the thermal ones are increased by 3-4 times thus they exceed significantly the former and become dominant source of neutrons. At the highest temperatures, nearly 60% of the total neutrons are generated by thermal fusion reactions. Record neutron baseline pulse #96482 for instance has only 38% BT neutrons.

For the hybrid pulses, similar trends are observed. N_{BT} increases with $T_e(0)$ and $T_i(0)$, but the ratio N_{BT}/N_{TOT} decreases from about ≈80% at lowest temperature to about ≈55% for the highest central temperatures. The latter indicates that even for the hybrid pulses, which rely considerably on BT neutrons, improvement in total neutron performance with $T_i(0)$ is mainly due to enhancement in thermal rates.

The result of the analysis of BT neutrons and the ratio of central ion and electron temperatures $T_i(0)/T_e(0)$ is shown in figure 12.

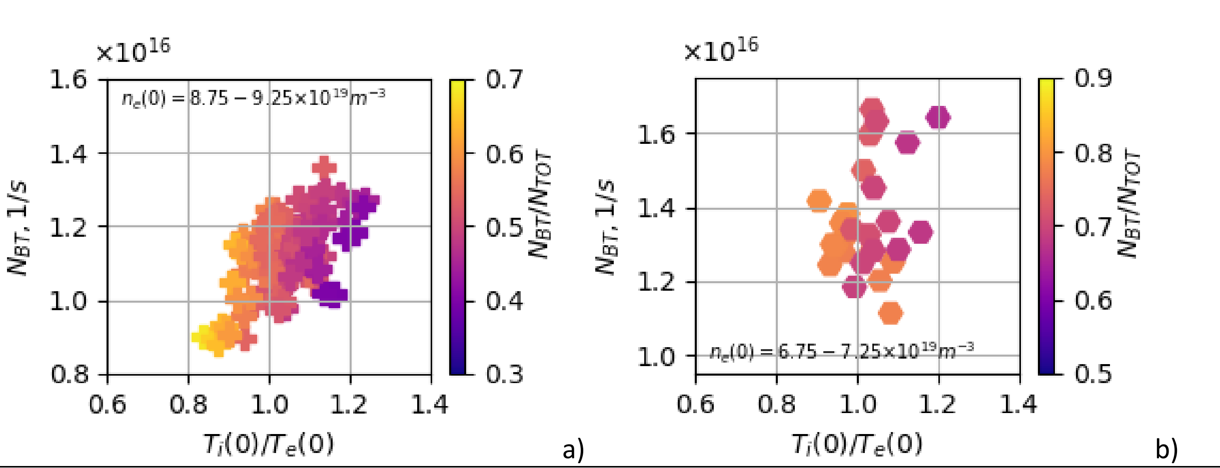

Figure 12: BT neutrons, N_{BT}, versus the ratio of central ion and electron temperatures $T_i(0)/T_e(0)$ for 3.3T/3.5MA with $n_e(0)=8.75\text{-}9.25\times10^{19}m^{-3}$ baseline pulses a) and 2.8-3.4T/2.15MA hybrid pulses with $n_e(0)=6.75\text{-}7.25\times10^{19}m^{-3}$ b). Colour mapped symbols show ratio of BT neutrons to total calculated neutrons, N_{BT}/N_{TOT}.

BT neutrons, N_{BT}, increase with $T_i(0)/T_e(0)$ for both baseline and hybrid pulses as shown in figure 12. Total counts, N_{TOT}, also increase with $T_i(0)/T_e(0)$ as well as the contribution from the thermal neutrons. The latter can be deduced from the reduction in the ratio N_{BT}/N_{TOT} shown by colour mapped symbols in figure 12. This observation is fully consistent with discussions in [13]. What is shown in addition here is that for both baseline and hybrid cases the higher the $T_i(0)/T_e(0)$ ratio is the higher the thermal and BT neutrons are. In our case, high performance with large fraction of thermal yield, $N_{TOT}>4\times10^{16}$ 1/s and $N_{TH}/N_{TOT}\approx0.7$, is clearly achieved for conditions close to hot ion mode with $T_i(0)/T_e(0)>1.2$. In conditions $T_i(0)/T_e(0)<0.9$ both total and BT yield decrease while the thermal fraction reduces significantly as $N_{BT}/N_{TOT}\approx0.7\text{-}0.8$. It is difficult to discuss the implications of this conclusion regarding DT fusion plasma where $T_i(0)/T_e(0)<1$ is expected [6]. The complete analysis of this problem would require self-consistent transport modelling taking into account the alpha particle heating [45] which is beyond the scope of the present analysis.

5.3 Synergistic effects

The impact of the synergistic effects was studied in detail during the previous JET campaign [16], [17]. Synergistic effects are further studied here for the higher density pulses of the latest JET campaign. This is done by means of comparing a pair of TRANSP runs: one with RF power and RF kick operator, while the other one was performed with RF kick operator turned off. For the baseline scenario, the record JET pulse #96482 was selected and results are shown in figure 13.

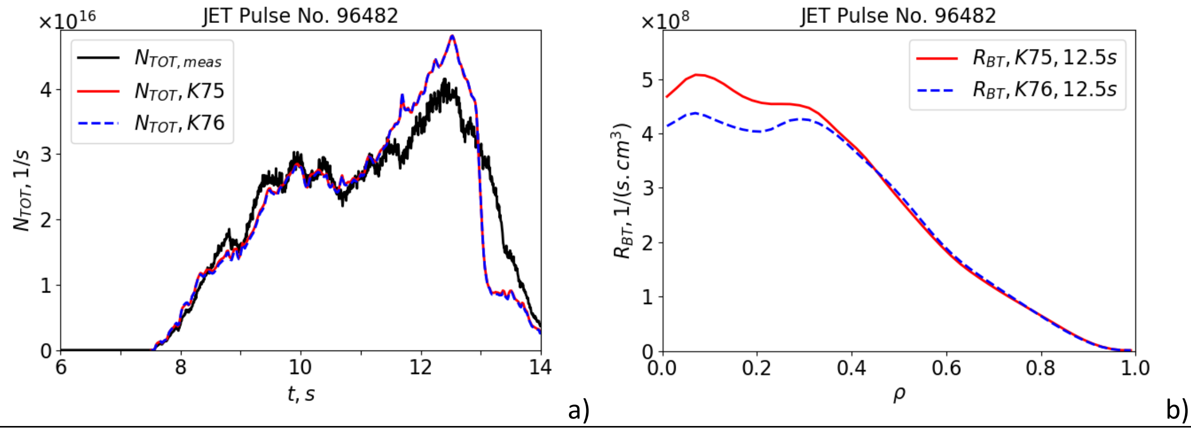

Figure 13: Total neutron count N_{TOT} in a) and BT neutron rates R_{BT} at 12.5s in b) for JET pulse #96482 modelled by TRANSP with RF power and RF kick operator (red lines) and with RF kick operator turned off (blue dashed lines). Experimental total neutron count (black lines) is provided in a) for comparison.

Comparing directly the neutron counts with and without synergistic effects, figure 13 a), it seems that the impact is negligible. In figure 13 b), shown are BT neutron rates profiles, $R_{BT}(\rho)$, at the maximum performance time t=12.5s in both cases. The increase in BT rates for $\rho<0.4$ in the case with synergistic effects shows that they have only small effect in the core. The small volume of this region is however not sufficient to contribute significantly to detectable increase in total neutron yield.

Fast ions densities, $n_{fi}(R,Z)$, and distribution function in the plasma centre, $f_D(v_{parl},v_{perp})$ at R=3.02m, Z=0.31m or $\rho=0$, for the two cases discussed above are shown in figure 14.

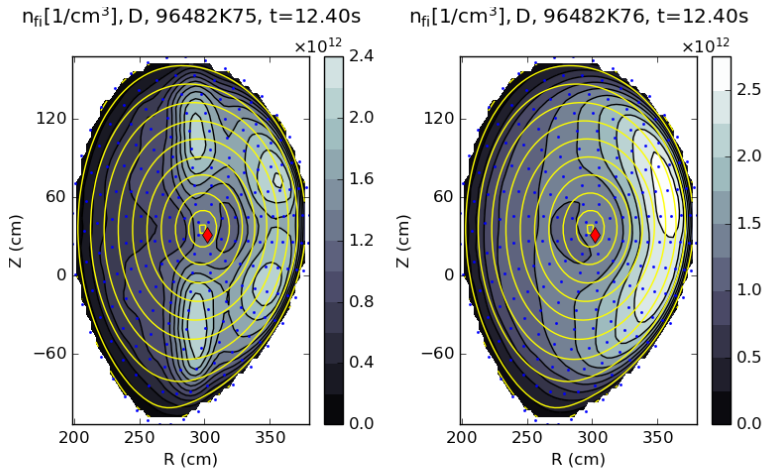

a)

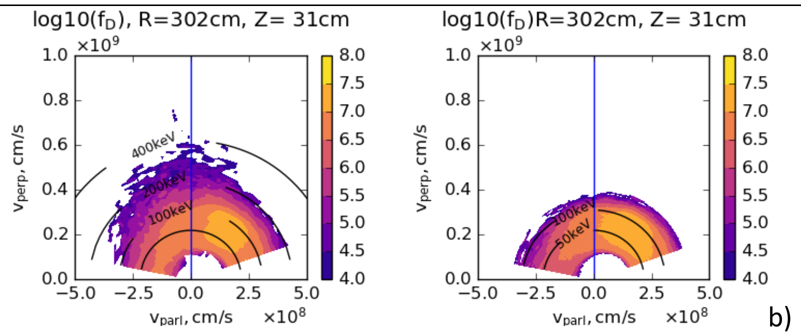

Figure 14: Fast ions densities $n_{fi}(R,Z)$ in a) and distribution function $f_D(v_{parl},v_{perp})$ in the plasma centre, at t=12.4s and at R=3.02m, Z=0.31m or ρ=0 in b) for JET pulse #96482 modelled by TRANSP with RF power and RF kick operator (left figures, TRANSP run K75) and with RF kick operator turned off (right figures, TRANSP run K76).

Synergy effect are clearly present as it can be seen from the modifications of fast ions distribution function in the core, figure 14 b) left graph vs. right graph. It is worth noting that NB fast ions density is very off-axis and poloidally asymmetric and peaked on the LFS, figure 14 a). The small modification of fast ions distribution function for the case with RF kick operator, figure 14 b) left graph vs. right graph, confirm that synergistic effects have small impact on the neutron rates in the core. This is due to lower fast ions density near Doppler shifted resonance region in the core. The last statement can be confirmed after comparing against old JET pulse #92436 where synergy effects were assessed [17] to contribute to total neutron count by ≈5%. The difference between these two cases is that in the lower density pulse #92436 beam deposition and fast ions density are very central, so when turning on RF fast ions, density is higher in Doppler shifted resonance region and as a result synergy effects are more pronounced.

For the hybrid pulses the picture is very similar. Record neutron yield pulse #96947 is investigated for the impact of synergistic effects by having two TRANSP runs: one with RF power and RF kick operator, while the other one was performed with RF kick operator turned off. Difference in total neutrons is again very negligible. Synergistic effects are still present but to a very small extent in the core, for ρ <0.3. This is however accompanied by reduction of BT rates for ρ >0.3 as the total effect is practically negligible.

6 Conclusions

The analysis presented here shows that despite the negative impact of higher core density and density peaking on beam penetration the fusion performance and the total neutrons are in fact improved due to achieving higher core temperatures and thermal reactions. In both scenario, baseline and hybrid, the thermal DD fusion gain, assessed here by means of the ratio N_{TH}/P_{LOSS} is linear with β_N and $B_t\tau$ thus fully in agreement with triple product scaling [7]. The total fusion gain, N_{TOT}/P_{LOSS}, however, is more scattered and inconsistent with expected linear scaling with normalised beta and confinement time. This discrepancy is attributed to the contribution of BT reactions.

Central electron density and density peaking have negative impact on the beam penetration and central fast ions density. BT neutrons are, however, not affected by this and can even benefit from conditions with higher central temperatures. The importance of achieving higher core temperatures is further highlighted not only by the fact that higher total neutron yield can be reached but also a higher ratio of thermal to total neutrons can be attained. The analysis of JET's high performance pulses also indicates that having $T_i(0)/T_e(0)>1.2$ favours total and thermal neutrons, whilst for ITER operational space with $T_i(0)/T_e(0)<1$ total and BT neutrons would be expected to decrease.

Synergistic effects are assessed to have negligible effect in conditions of higher density restricting NB penetration. This conclusion somewhat differs from earlier observations [17] where about 5% and 10% enhancement in DD neutrons was reported for baseline and hybrid pulses. This discrepancy can be explained with the higher density attained in the more recent baseline pulses, with line averaged density of about $7.6\times10^{19}m^{-3}$ in #96482 compared to $6.4\times10^{19}m^{-3}$ in #92436. This results in very peripheral beam penetration and lower fast ions density in the core, figure 14 a), hence weaker synergistic effects.

7 Acknowledgement

This work has been carried out within the framework of the EUROfusion Consortium and has received funding from the Euratom research and training programme 2014-2018 and 2019-2020 under grant agreement No 633053. The views and opinions expressed herein do not necessarily reflect those of the European Commission.

8 References

[1] ITER Physics Basis Editors et all, 1999 Nucl. Fusion 39 2137
[2] M. Shimada et al, 2007 Nucl. Fusion 47 S1
[3] ITER Physics Expert Group on Energetic Particles Heating and Current Drive, 1999 Nucl. Fusion 39, 2495
[4] D.L. Jassby, 1977 Nucl. Fusion 17 309
[5] ITER Physics Expert Groups on Confinement and Transport and Confinement Modelling and Database, 1999 Nucl. Fusion 39 2175
[6] E. J. Doyle et al 2007, Nucl. Fusion 47, p. S18
[7] C. C. Petty, 2008 Phys. Plasmas 15, 080501
[8] J. Wesson, 2011, Tokamaks, 4th edition, Oxford University press
[9] M. Kikuchi, K. Lackner, M. Q. Tran, 2012, Fusion physics, Vienna: International Atomic Energy Agency
[10] H.-S. Bosch and G.M. Hale, 1992 Nucl. Fusion 32 611
[11] M. Mikkelsen et al, 1989 Nucl. Fusion 29 1113
[12] E. Joffrin et al, 2019 Nucl. Fusion 59 112021
[13] Hyun-Tae Kim et al, 2018 Nucl. Fusion 58 036020
[14] JET team, 1992, Nucl. Fusion 32 187
[15] M. Mantsinen et al 2017 Eur. J. Phys. 157 03032
[16] D. Gallart et al 2018 Nucl. Fusion 58 106037
[17] K.K. Kirov et al 2019 Nucl. Fusion 59 056005
[18] I. Nunes et al 2016 Plasma Phys. Control. Fusion 58 014034
[19] L. Garzotti et al 2019 Nucl. Fusion 59 076037
[20] A.C.C. Sips et al 2018 Nucl. Fusion 58 126010
[21] C.D. Challis et al 2015 Nucl. Fusion 55 053031
[22] J. Garcia et al 2015 Nucl. Fusion 55 053007
[23] J. Citrin et al 2013 Phys. Rev. Lett. 111 155001
[24] A.R. Polevoi et al 2002 J. Plasma Fusion Res. Ser. 5 82
[25] G.V. Pereverzev et al 2005 Nucl. Fusion 45 221
[26] M.B. Isichenko et al 1996 Phys. Rev. Lett. 74 4436

[27] R.J. Hawryluk et al "An Empirical Approach to Tokamak Transport", in Physics of Plasmas Close to Thermonuclear Conditions, ed. by B. Coppi, et al., (CEC, Brussels, 1980), Vol. 1, pp. 19-46
[28] R. V. Budny, M. G. Bell, H. Biglari, et al.1992, Nucl Fusion 32, p.429.
[29] http://w3.pppl.gov/transp
[30] B. A. Grierson et al 2018, Fus. Sci. Techn., DOI: 10.1080/15361055.2017.1398585
[31] A. Pankin, D. McCune, R. Andre et al., "The Tokamak Monte Carlo Fast Ion Module NUBEAM in the National Transport Code Collaboration Library", Computer Physics Communications Vol. 159, No. 3 (2004) 157-184.
[32] M. Brambilla 1999, Plasma Phys. Control. Fusion 41, p.1
[33] J-M Kwon et al 2006 Bulletin of the American Physical Society, 48th meeting of the Division of Plasma Physics, Philadelphia (PA) (2006), Development of XGC-RF for Global Guiding-Center Particle Simulation of minority ICRH heated Plasmas in a General Tokamak Geometry
[34] J-M Kwon et al 2007 Bulletin of the American Physical Society, 49th meeting of the Division of Plasma Physics, Orlando (FL) (2007), Enhancement of NUBEAM for the simulation of fast ion and RF-wave interaction based on the quasi-linear theory
[35] R. Budny, M. Gorelenkova 2015 57th Annual Meeting of the APS Division of Plasma Physics, Volume 60, Number 19, GP12.00127, 16–20 Nov 2015, Savannah, Georgia
[36] C. Gowers et al 1995 Rev. Sci. Instrum. 66 471
[37] E. de la Luna et al 2001 Rev. Sci. Instrum. 74 1414
[38] L.C. Ingesson, 1999 Comparison of methods to determine the total radiated power in JET, JET Report JET-R(99)06
[39] V. Zoita et al. 2009, "Neutron fluence measurements on the JET tokamak by means of super-heated fluid detectors," 2009 IEEE International Conference on Plasma Science - Abstracts, San Diego, CA, 2009, pp. 1-1, doi: 10.1109/PLASMA.2009.5227402.
[40] T.M. Biewer et al 2007, "Charge Exchange Recombination Spectroscopy Measurements from Multiple Ion Species on JET", JET report EFDA–JET–CP(07)03/24
[41] M. Gatu Johnson et al 2008 Nucl. Intrum. Methods A **591** 417
[42] C. Hellesen et al 2010, Plasma Phys. Control. Fusion 52 085013
[43] [A. Hjalmarsson, Development and Construction of a 2.5-MeV Neutron Time-of-Flight Spectrometer Optimized for Rate (TOFOR). PhD thesis, Uppsala University, Department of Neutron Research, 2006, http://urn.kb.se/resolve?urn=urn%3Anbn%3Ase%3Auu%3Adiva-7198]
[44] J.M. Adams, 1993 Nuclear Instruments and Methods in Physics Research A329 (1993) 277-290
[45] J. Garcia et al 2019 Nucl. Fusion 59 086047
[46] T.H. Stix, 1972, Plasma Physics, Vol. 14, pp. 367
[47] K. K. Kirov et al 2019, 23rd Topical Conference on Radiofrequency Power in Plasmas (RFPPC 2019), 14–17 May 2019, Hefei, China
[48] K. Miyamoto, 2016, Plasma Physics for Controlled Nuclear Fusion, 2nd edition, Springer-Verlag Berlin Heidelberg
[49] K. Miyamoto, 2000, J. Plasma Fusion Res. **76** 166